

Stigmastane-type steroids with unique conjugated $\Delta^{7,9(11)}$ diene and highly oxygenated side chains from the twigs of *Vernonia amygdalina*

Xiangzhong Liu¹, Wenjing Tian¹, Guanghui Wang, Qiannan Xu, Mi Zhou, Shuo Gao, Daren Qiu, Xin Jiang, Cuiling Sun, Rong Ding, Ting Lin^{**}, Haifeng Chen^{*}

Fujian Provincial Key Laboratory of Innovative Drug Target, School of Pharmaceutical Sciences, Xiamen University, Xiamen, 361005, PR China

ARTICLE INFO

Keywords:

Vernonia amygdalina Delile (compositae)
Stigmastane-type steroids
Absolute configuration
RXR α
NF- κ B

ABSTRACT

Veramyosides A–J, eleven undescribed stigmastane-type steroids, including one aglycone and ten glycosides, along with three known homologues were isolated from the twigs of *Vernonia amygdalina* Delile (compositae). All compounds featured a stigmastane-type steroid skeleton with a unique conjugated $\Delta^{7,9(11)}$ diene segment and highly oxygenated side chains with a γ -lactone or an α , β -unsaturated five-membered lactone ring. The structures of veramyosides A–J and their absolute configurations were unambiguously elucidated by HR-ESI-MS, extensive NMR spectroscopy, in situ dimolybdenum CD methods, modified Mosher's method, quantum chemical calculation of their ECD curves, and CD comparison methods on basis of their biogenetic pathway. In addition, all isolates were investigated for their effects on RXR α transcription, and their effects on the NF- κ B signaling pathway were also evaluated.

1. Introduction

Stigmastane-type steroids, a family of phytosterols, are structurally characterized by the presence of 1,2-cyclopentanoperhydrophenanthrene ring system composed of 17 carbon atoms arranged in four rings and 10 carbon atoms in side chains. The core structures of stigmastane-type steroids can be classified into two categories that differ from each other by the position of the conjugated diene, at $\Delta^{7,9(11)}$ or $\Delta^{8,9(14)}$. Nevertheless, only a few $\Delta^{7,9(11)}$ stigmastane-type steroids have been reported, and they were primarily found in the genus *Vernonia*. The reported $\Delta^{7,9(11)}$ stigmastane-type steroids were characterized by highly oxidized side chains with 21, 23-epoxy, 22, 24-epoxy or other cyclized moieties as well as polyhydric substituted acyclic fragments, and these compounds showed a vast array of biological activities, such as anti-malarial, antimicrobial, anthelmintic and antithrombotic activities (Audu et al., 2012). Modifications of side chains with different cyclization patterns, attached groups and configurations led to the structural diversity of $\Delta^{7,9(11)}$ stigmastane-type steroids. Thus, the $\Delta^{7,9(11)}$ stigmastane-type steroids can be considered as a rich source of undescribed structures and active lead compounds.

Vernonia amygdalina Delile (Compositae), a member of the genus *Vernonia*, shows great efficacy in the treatment of gout, amoebic

dysentery, gastrointestinal disorders and so on. Two major categories of constituents, steroids and sesquiterpene lactones, were found in *V. amygdalina* and were reported to have activities including antimalarial (Nerdy, 2015), anti-breast cancer (Luo et al., 2011; Yedjou and Tchounwou, 2017), and anti-nasopharyngeal carcinoma activities (Kupchan et al., 1969). However, the $\Delta^{7,9(11)}$ stigmastane-type steroids were the most common steroids in *V. amygdalina*, with only 20 distinct compounds discovered (Ohigashi et al., 1991; Jisaka et al., 1992, 1993; Kamperdick et al., 1992; Igile et al., 1995; Schmittmann et al., 1994; Quasie et al., 2016; Wang et al., 2018), which shows great potential in medicinal chemistry study of this plant. In our efforts to find more active $\Delta^{7,9(11)}$ stigmastane-type steroids with undescribed structures, eleven undescribed $\Delta^{7,9(11)}$ stigmastane-type steroids along with three known steroids (Fig. 1) were isolated from the twigs of *V. amygdalina*. Compounds 1–11 featured a $\Delta^{7,9(11)}$ stigmastane-type steroid skeleton with highly oxygenated side chains characterized by the existence of a 21, 23-epoxy bridge leading to the formation of a γ -lactone or an α , β -unsaturated five-membered lactone ring. Herein, we report the isolation, structural elucidation, and biological evaluation of the isolated compounds.

* Corresponding author.

** Corresponding author.

E-mail addresses: linting@xmu.edu.cn (T. Lin), haifeng@xmu.edu.cn (H. Chen).

¹ These two authors contributed equally to this research.

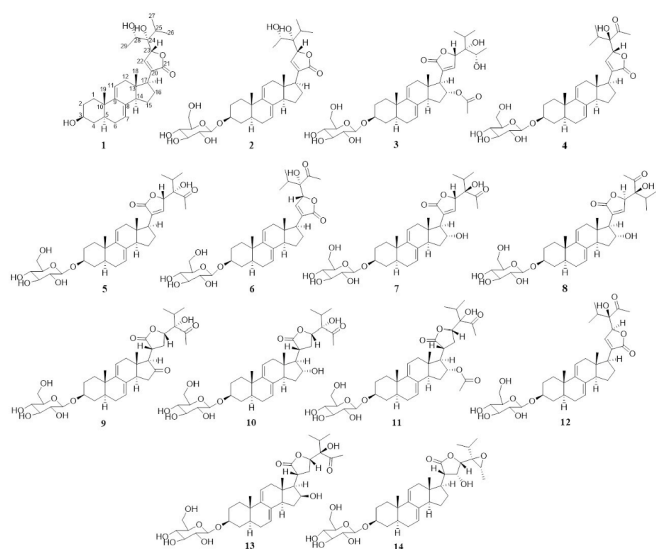


Fig. 1. Chemical structures of veramyosides A–J (1–14).

2. Results and discussion

2.1. Isolation and structural elucidation

The powdered twigs of *V. amygdalina* were extracted with 60% EtOH(aq.) and partitioned consecutively with petroleum ether, dichloromethane, ethyl acetate and *n*-butyl alcohol. The dichloromethane extract was repeatedly separated by a variety of chromatographic methods to afford eleven undescribed (1–11) and three known (12–14) stigmastane-type steroids (Fig. 1).

Veramyoside A (1), [α] $_{D}^{25}$ -40.00 (*c* 1.30, CH₃OH), was obtained as an amorphous white powder. Its molecular formula was assigned as C₂₉H₄₂O₅ based on its HR-ESI-MS data with a pseudo molecular ion at *m/z* 493.2921 [M + Na]⁺ in the positive mode, corresponding to 9 indices of hydrogen deficiency. The absorption bands at 3411, 1738, and 1641 cm⁻¹ in its IR spectrum suggested the presence of hydroxy groups, an ester carbonyl and olefinic functionalities. The ¹H NMR spectrum shows three olefinic protons [δ _H 7.52 (1H, t, *J* = 1.4 Hz), 5.53 (1H, d, *J* = 6.5 Hz) and 5.46 (1H, br. s)], an isopropyl group [1.03 (3H, d, *J* = 7.1) and 0.99 (3H, d, *J* = 7.0)], two angular methyls [0.91 (3H, s) and 0.47 (3H, s)] and another methyl [1.30 (3H, d, *J* = 6.6 Hz)]. The ¹³C NMR and DEPT spectra exhibited 29 carbon resonances, including the signals characteristic of a carbonyl [δ _C 176.5], six olefinic carbons [δ _C 151.9, 145.5, 137.3, 134.8, 121.9, and 119.6] and five methyl carbons [δ _C 19.8, 18.7, 18.7, 18.6, and 13.0]. The above analysis indicated that 1 was a derivative of a stigmastane-type steroid. In addition, the characteristic UV absorptions at 234, 243, and 250 nm suggested the existence of a unique conjugated $\Delta^{7,9(11)}$ moiety in the steroid core, which are present in $\Delta^{7,9(11)}$ stigmastane-type steroids, which was further confirmed by the HMBC correlations (Fig. 2). The

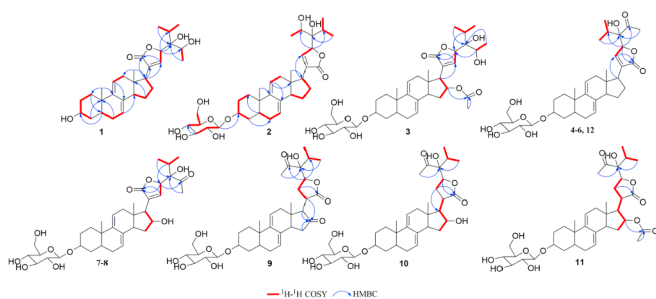


Fig. 2. Key HMBC correlations of 1–11.

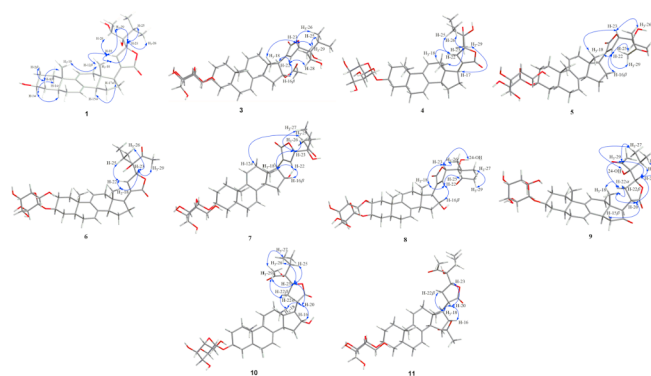


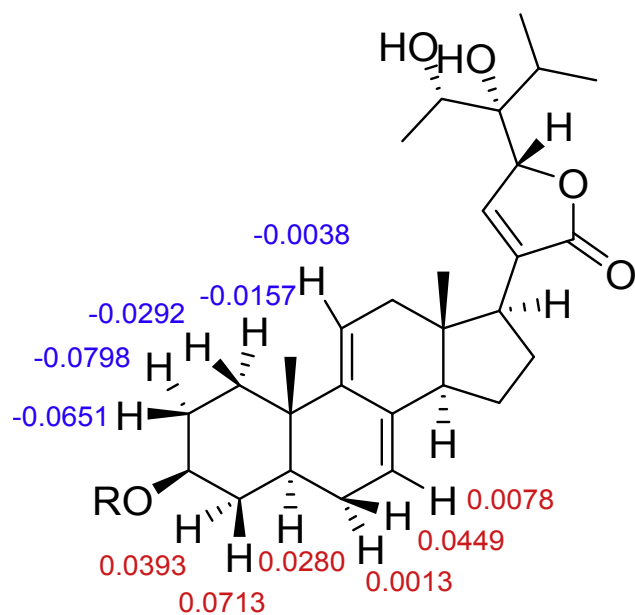
Fig. 3. Key NOESY correlations of 1–11.

$\Delta^{7,9(11)}$ stigmastane-type steroid core accounts for 6 degrees of unsaturation, and the remaining 3 degrees of unsaturation and the remaining C₁₀H₁₆O₄ in the side chains indicated the presence of one olefin, one carbonyl and an additional ring. The ¹H–¹H COSY correlations of H-22/H-23 and the HMBC correlations from H-22 to C-21 and from H-23 to C-20/C-21 suggested that C-21 and C-23 were linked via an oxygen bridge to form an α , β -unsaturated five-membered lactone ring (Fig. 2). The ¹H–¹H COSY correlations of H-25/H₃-26, H-25/H₃-27 and H-28/H₃-29 as well as the HMBC correlations from H-23 to C-24/C-25/C-28, from H₃-26 to C-24, and from H-28 to C-24, together with the chemical shifts of C-24 (δ _C 79.7) and C-28 (δ _C 71.3) indicated the presence of a 1,2-OH-1-isopropyl-propyl group, which was connected to the lactone ring at C-23 and C-24 (Fig. 2). In addition, the HMBC correlations from H-17 to C-20/C-21/C-22 constructed the linkage of the side chain to C-17 of the steroid core (Fig. 2). Thus, the planar structure of 1 was deduced.

The relative configuration of 1 was determined by a NOESY experiment (Fig. 3). The NOESY correlations of H-1 α /H-3/H-5, H-2 β /H₃-19/H-4 β , H₃-19/H₃-18/H-15 β and H-17/H-14 suggested the *trans* fusion of the A/B and C/D rings and the β -orientation of OH-3, CH₃-19, CH₃-18 and the C-17 side chain. Additionally, the NOESY correlations of H-22/H-12 β , H-22/H₃-18 and H-23/H₃-18 indicated the relative position of lactone ring E and the β -orientation of H-23. The relative configurations of C-24 and C-28 were deduced from the NOESY correlations of H-23/H-25, H-23/H-26, H-22/H-28, H-22/H-29, H-23/H-28 and H-23/H-29.

The absolute configuration of C-3 was determined by a modified Mosher's method (Tian et al., 2016; Ohtani et al., 1991). The $\Delta\delta$ values between the (S) and (R)-MTPA esters indicated the S configuration for C-3 (Fig. 4). In addition, the absolute configurations of the *vic*-diols at C-24 and C-28 were determined by the in situ dimolybdenum CD method (Bari et al., 2001; Marcin et al., 2007; Liu et al., 2010). According to the empirical rule proposed by Sznatzke, the negative Cotton effect at approximately 400 nm (Fig. 5) observed in the induced CD spectrum permitted the assignment of the absolute configuration of the *vic*-diol as 24S, 28R. Consequently, the absolute configuration of 1 was established as 3S, 5R, 10S, 13S, 14R, 17S, 23R, 24S, 28R.

Veramyoside B (2), an amorphous white powder, gave the molecular formula C₃₅H₅₂O₁₀, corresponding to 10 degrees of unsaturation, as revealed by its HR-ESI-MS signal at *m/z* 655.3441 [M + Na]⁺ (calcd. 655.3453). Both the 1D and 2D NMR data of 2 were similar to those of 1, except for the presence of a glucosyl group [δ _C 102.6, 79.1, 78.9, 75.8, 72.1, and 63.3], which accounted for the additional one degree of unsaturation. (Fig. 2). The β orientation of the anomeric proton was assigned based on the *J*_{1H,2H} value coupling constant (*J* = 7.7 Hz) (Ma et al., 2016). The absolute configuration of the sugar moiety was determined as β -D-glucose by HPLC analysis of its derivative after acid hydrolysis (Ye et al., 2017; Tanaka et al., 2007; Niu et al., 2017). The HMBC correlation from H-1' to C-3 indicated that the β -D glucosyl group was linked to C-3 of the core structure, which was



$$\Delta\delta \text{ values (in ppm)} = \delta_S - \delta_R \text{ (A-B)}$$

Fig. 4. $\Delta\delta$ values (in ppm) = $\delta_S - \delta_R$ for the (S)- and (R)-MTPA esters (A and B) of **1**.

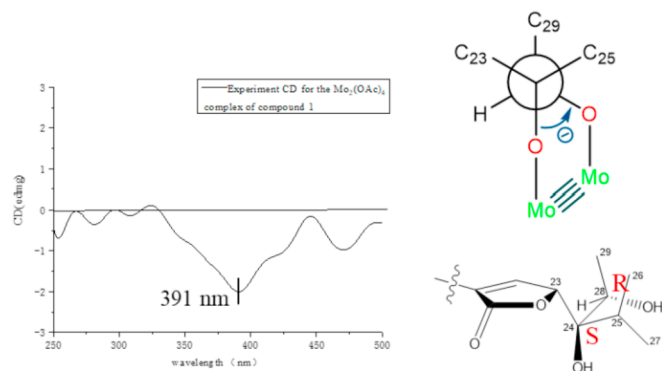


Fig. 5. $\text{Mo}_2(\text{OAc})_4$ -induced ECD spectrum of **1** and a Newman projection of the diol moiety of **1**, with the helicity rule applied.

further confirmed by the glycosidation shifts in the resonances of C-2 (δ_C 30.5) and C-4 (δ_C 34.9) (Fig. 2). The relative configurations of the chiral centers at C-3, C-5, C-10, C-13, C-14, C-17, C-23, C-24, and C-28 in **2** were consistent with those of **1** on the basis of their NOESY data.

The ECD curve of **2** is a highly consistent with that of biogenetically related compound **1**, which indicates that these two compounds have the same absolute configuration (Fig. 7). Therefore, the absolute configuration of **2** was defined as 3S, 5R, 10S, 13S, 14R, 17S, 23R, 24S, 28R.

Veramyoside C (**3**) was isolated as a white solid. Its molecular formula was determined as $\text{C}_{37}\text{H}_{54}\text{O}_{12}$ according to its molecular ion $[\text{M} + \text{Na}]^+$ at m/z 713.3415 in the HR-ESI-MS. Extensive analysis of its NMR data revealed that **3** was closely related to **2** except for an additional acetoxy substituent [δ_C 171.1 and 21.3] at C-16, which was further confirmed by the obvious downfield shift of C-16 (δ_C 77.9) and the HMBC correlations from H-16 (δ_H 6.03) to C-1' (δ_C 171.1) and from H₃-2'' (δ_H 1.98) to C-1' (δ_C 171.1). According to the NOESY spectrum, the relative configurations of C-3, C-5, C-10, C-13, C-14, and C-17 in **3** were identical to those of **2**. In addition, the NOESY correlations of H-22/H₃-18 and H-22/H-16 β suggested the relative position of the D/E rings and the α -orientation of the acetoxy unit. The NOESY cross-peaks between H-23 and H₃-18 indicated that H-23 was β -oriented. In addition, the relative configurations of C-24 and C-28 were deduced by the NOESY correlations (Fig. 3) of H-23/H-28, H-22/H₃-29, H-23/H₃-26 and H-25/H₃-29. The experimental ECD curves of **3** and **2** showed the same Cotton effects (Fig. 7), which allowed the assignment of the absolute configuration of **3** as 3S, 5R, 10S, 13S, 16R, 17R, 23S, 24R, 28S.

Veramyoside D-F (**4–6**) were obtained as amorphous white powders with the same molecular formula, $\text{C}_{35}\text{H}_{50}\text{O}_{10}$, identified by their HR-ESI-MS data. The IR, UV, and NMR data of **4–6** were identical to those of known compound **12**, which has the same planar structure, and this assignment was further confirmed by their $^1\text{H}-^1\text{H}$ COSY and HMBC spectra (Fig. 2). A thorough comparison of the NMR data of these four compounds suggested that they were stereoisomers with variations in the configurations at C-23 and C-24, as proved by the differences in the NOESY correlations of their side chains. In the NOESY spectrum of **4**, the correlations of H₃-27/H-23/H₃-18/H-22/H-25 and H₃-29/H-17 allowed the determination of the relative configurations of C-23 and C-24 as (23R*, 24R*), as shown in Fig. 3. The relative configurations of C-23 and C-24 in **5** were established as (23S*, 24S*) by the NOESY correlations of H₃-18/H-22/H-16 β , H₃-18/H-23/H₃-26 and H-25/H-22/H₃-29. Similarly, the NOESY correlations of H₃-18/H-23, H₃-18/H-22/H-25 and H₃-27/H-23/H₃-29 in **6** indicated the relative configurations of C-23 and C-24 as 23R*, 24S* (Fig. 3). The relative configuration of these two chiral carbons in known compound **12** was reported by Wang J as 23S*, 24R* (Wang et al., 2018). Thus, these four compounds accounted for all the possibilities of the configurations of C-23 and C-24: (23R*, 24R*)-**4**; (23R*, 24S*)-**5**; (23S*, 24S*)-**6**; and (23S*, 24R*)-**12**.

The absolute configuration of **4** was determined by calculating its ECD curve. Based on the deduced relative configurations, the ECD spectra of (3S, 5R, 10S, 13S, 17S, 23R, 24R)-**4** was calculated. As a result, the overall pattern of its experimental ECD curve was highly consistent with the calculated curve. Thus, the absolute configuration of **4** was assigned as 3S, 5R, 10S, 13S, 17S, 23R, 24R. Additionally,

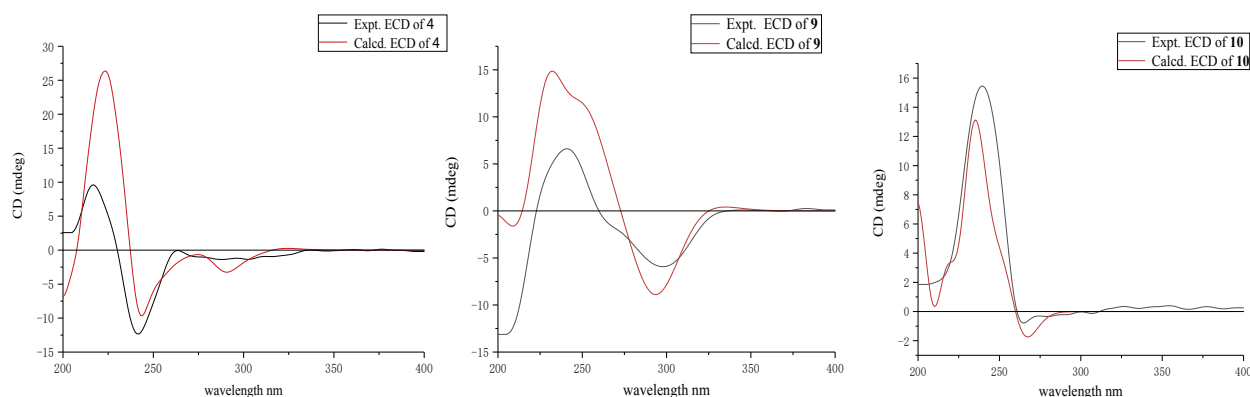


Fig. 6. Experimental and calculated ECD spectra of **4**, **9** and **10**.

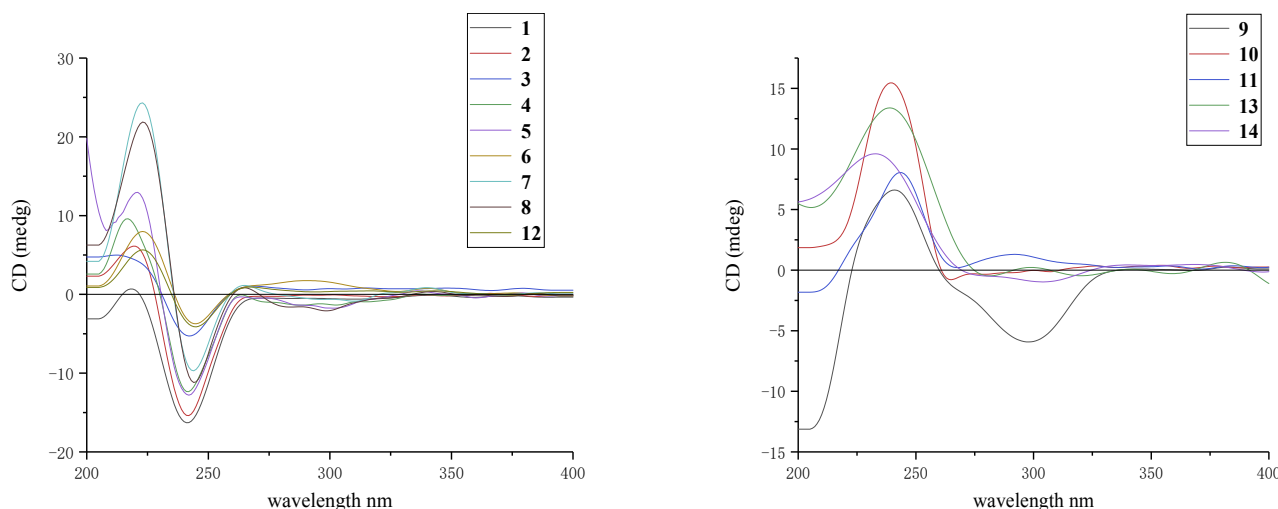


Fig. 7. Comparison of the experimental ECD spectra of 1–14.

considering the biogenetic relationship among these compounds, the absolute configurations of **5**, **6** and **12** were determined as (3*S*, 5*R*, 10*S*, 13*S*, 17*S*, 23*S*, 24*S*), (3*S*, 5*R*, 10*S*, 13*S*, 17*S*, 23*R*, 24*S*) and (3*S*, 5*R*, 10*S*, 13*S*, 17*S*, 23*S*, 24*R*), respectively, based on a comparison of their Cotton effects with the ECD spectrum of **4** (Fig. 7).

Veramyoside H (**7**) and veramyoside I (**8**), amorphous white powders, gave the same molecular formula, C₃₅H₅₀O₁₁, based on their HR-ESI-MS data, with an additional oxygen compared with the molecular formula (C₃₅H₅₀O₁₀) of **4–6**. Careful comparison of their NMR data revealed that **7** and **8** were structural analogues of **4–6** except for the hydrogen at C-16 in **4–6** was substituted by a hydroxyl group in **7** and **8** based on the obvious downfield shift of C-16 (δ_C 76.0) in **7** and C-16 (δ_C 74.3) in **8**. Their planar structures were further confirmed by their ¹H-¹H COSY and HMBC spectra (Fig. 2). The NOESY spectra (Fig. 3) of **7** and **8** both showed correlations of H₃-18/H-22/H-16 suggesting that H-16 in each of these two compounds was β -oriented. The relative configurations of C-23 and C-24 in **7** and **8** were deduced as (23*S**, 24*R**)-**7** and (23*R**, 24*S**)-**8** from their NOESY spectra (Fig. 3), and these configurations are identical to **6** and **12**, respectively. The CD spectra of **7** and **8** showed the same Cotton effects as those of biogenetically related compound **4** (Fig. 7). Thus, the absolute configurations of **7** and **8** were unambiguously determined as 3*S*, 5*R*, 10*S*, 13*S*, 14*R*, 16*R*, 17*S*, 23*S*, 24*R* and 3*S*, 5*R*, 10*S*, 13*S*, 14*R*, 16*R*, 17*S*, 23*R*, 24*S*, respectively.

Veramyoside J (**9**) was isolated as an amorphous white powder, with the same molecular formula (C₃₅H₅₀O₁₁) as **7** and **8** as deduced from its HR-ESI-MS data (molecular ion [M + Na]⁺ detected at *m/z* 653.3204). The NMR data of **9** were identical to those of **7** and **8** except for the obvious upfield shift of C-20 (δ_C 38.2) and C-22 (δ_C 27.4) as well as a significant downfield shift of C-16 (δ_C 214.6), which suggested the hydrogenation of the C=C bond between C₂₀ and C₂₂ as well as the oxidation of 16-OH to a carbonyl. These assignments were further confirmed by the ¹H-¹H COSY correlations of H-20/H-22 and the HMBC correlations from H-17/H-20 to C-16 (Fig. 2). The relative configuration of **9** was determined from its NOESY spectrum (Fig. 3). The β -orientations of H-20 and H-23 were deduced from the correlations of H₃-18/H-20 and H-20/H-23. The relative configuration of C-24 was assigned based on the NOESY correlations of H-23/H₃-27, H-23/H-25, H₃-18/H-22 β , H-22 α /H₃-29 and H-22 α /24-OH. Based on the deduced relative configurations, the ECD curve of (3*S*, 5*R*, 10*S*, 13*S*, 14*R*, 20*R*, 23*S*, 24*S*)-**9** was calculated, which matched well with the experimental ECD curve of **9** (Fig. 6). Consequently, the absolute configuration of the **9** was defined as 3*S*, 5*R*, 10*S*, 13*S*, 14*R*, 20*R*, 23*S*, 24*S*.

Veramyoside K (**10**), an amorphous white powder, exhibited a molecular at ion *m/z* 647.3459 [M-H]⁻ in its HR-ESI-MS data, which suggested a molecular formula of C₃₅H₅₂O₁₁. Its ¹H and ¹³C NMR data

indicated that **10** was structurally similar to **9**. The obvious upfield shift of C-16 (δ_C 75.0) in **10** indicated that the carbonyl at C-16 in **9** had been converted to a hydroxy group. This conjecture was supported by the ¹H-¹H COSY correlations of H-15/H-16 and H-16/H-17 (Fig. 2). The relative configurations of C-20, C-23 and C-24 in the side chain of **10** were identical to those of **9** based on the similarities in their NOESY spectra (Fig. 3). The α -orientation of 16-OH was deduced by the NOESY correlation between H-20 and H-16. According to the deduced relative configurations, the ECD curve of (3*S*, 5*R*, 10*S*, 13*S*, 14*R*, 17*R*, 20*R*, 23*S*, 24*S*)-**10** was calculated for. As a result, the overall pattern of the calculated and experimental ECD spectra of **10** show the same Cotton effect (Fig. 6). Thus, the absolute configuration of **10** was determined to be 3*S*, 5*R*, 10*S*, 13*S*, 14*R*, 17*R*, 20*R*, 23*S*, 24*S*.

Veramyoside L (**11**) was obtained as an amorphous white powder with the molecular formula C₃₇H₅₄O₁₂ as determined from its HR-ESI-MS data. Analyses of the NMR data of **10** and **11** indicated they had similar planar structures, except for the presence of an additional acetyl group in **11**. The ¹H-¹H COSY correlations of H-15/H-16 and H-16/H-17, in conjunction with the HMBC cross-peaks from H-16 to δ_C 171.2 suggested that the additional acetyl group was linked to C-16 of the core structure (Fig. 2). The relative configuration of **11** was identical to **10** based on their NOESY spectra (Fig. 3). Their consistent CD data combined with the biogenetic relationship between **11** and **10** suggested they shared the same absolute configuration (Fig. 7). Consequently, the absolute configuration of **11** was assigned as 3*S*, 5*R*, 10*S*, 13*S*, 14*R*, 17*R*, 20*R*, 23*S*, 24*S*.

The CD spectra of the isolated compounds could generally be separated into two groups (Fig. 7), which could be attributed to the distinguishing lactone unit as well as the different configurations and conformations in the side chains. According to the octant-sector rule (Zhang et al., 2018), Compounds **1–8** and **12** showed the first CD pattern with Cotton effects at 220 nm (positive) and 240 nm (negative), which were presumed to arise from the $\pi \rightarrow \pi^*$ electronic transition of the α , β -unsaturated lactone. Another ECD pattern, with a positive Cotton effect at 240 nm (compounds **9–11** and **13–14**) may be primarily attributed to the lactone moiety in the side chain. Compared with the CD spectra of **10–11** and **13–14**, the synergistic Cotton effects at 300 nm (negative) in the CD spectrum of **9** would be due to the $n \rightarrow \pi^*$ electronic transition of the additional carbonyl at C-16 (Fig. 8).

2.2. RXR α and NF- κ B transcriptional activities

Retinoid X receptor- α (RXR α), a unique intracellular target for pharmacologic interventions, regulates diverse biologic processes and can be considered an intriguing target for cancer therapies (Bloch,

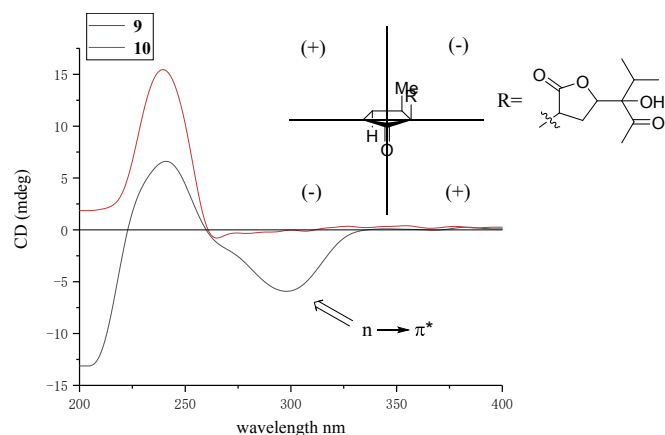


Fig. 8. Comparison of the experimental ECD spectra of **9** and **10**, and applying the octant rule to **9** accounts for the negative Cotton effect at approximately 300 nm.

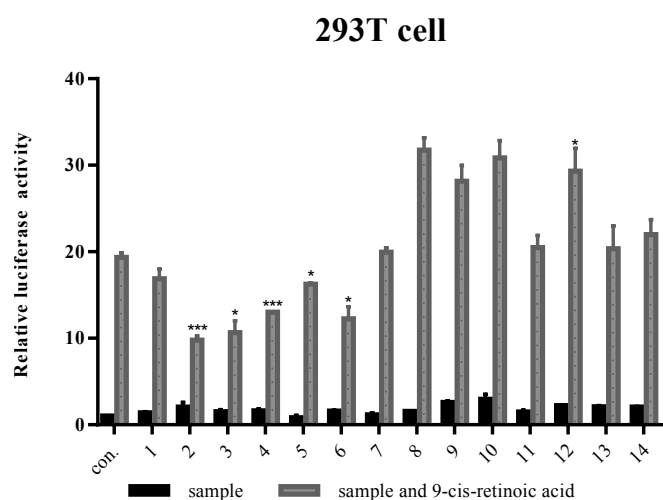


Fig. 9. Inhibition and activation effects of the isolates on RXR α transcription. Data are presented as the mean \pm SD, with * P < 0.05, *** P < 0.01 compared with the 9-cis group.

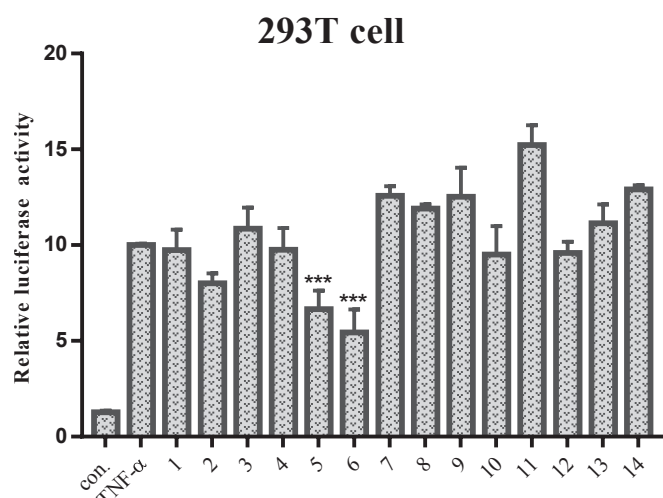


Fig. 10. Inhibitory effect of the isolates against the NF- κ B pathway. Data are presented as the mean \pm SD, with *** P < 0.01 compared with the TNF- α group.

1965). Some antagonists of RXR α can induce RXR α and Nur77 translocation from the nucleus to the cytoplasm, where they become

associated with Bcl-2 and execute proapoptotic effects (Cao et al., 2004; Zhou et al., 2014). Nuclear factor κ B (NF- κ B) is a family of transcription factors, that are also involved in the development and progression of cancer (Dolcet et al., 2005). TNF α can stimulate the NF- κ B and Akt pathways to enhance cell survival and provoke cancer cell apoptosis by activating the caspase-8-mediated death pathway under certain circumstances (Croft et al., 2013). Recently, studies have shown that some ligands of RXR α can inhibit TNF α activation of NF- κ B and promote cancer cell apoptosis. Thus, RXR α and NF- κ B could be considered therapeutic targets for the treatment of cancer (Zeng et al., 2015). All isolated compounds were investigated for their effects on the transcription of RXR α and NF- κ B. Compounds **2**, **3**, **4**, **5** and **6** could inhibit the 9-cis induced transcription of RXR α significantly compared with what was seen in the 9-cis group (* P < 0.05) (Fig. 9). In addition, compared with the TNF- α group, compounds **5** and **6** inhibited the NF- κ B pathway according to the dual luciferase reporter assay, and their effects were significant different (* P < 0.01) (Fig. 10). The preliminary structure-activity relationship analysis suggested that the $\Delta^{7,9(11)}$ stigmastane-type steroids with α , β -unsaturated lactone moieties in their side chains, except for compounds **7–8** with a hydroxyl group substituent at C-16, were more effective than compounds bearing a lactone moiety.

3. Conclusion

In conclusion, eleven undescribed stigmastane-type steroids, veramyosides A–J (**1–11**), along with three known homologues (**12–14**) were isolated from the twigs of *V. amygdalina*. Compounds **1–11** featured a $\Delta^{7,9(11)}$ stigmastane-type steroid skeleton with a unique conjugated $\Delta^{7,9(11)}$ diene segment and highly oxygenated side chains with a γ -lactone or an α , β -unsaturated five-membered lactone ring. Due to the flexible groups and multiple chiral centers in the side chains, determining the relative and absolute configurations of this type of compound is still a great challenge. In this paper, we have used the in situ dimolybdenum CD method, modified Mosher's method, quantum chemical calculation of their ECD and CD comparison methods combined with their biogenetic pathways to address these challenges. In addition, the effects of the compounds on the transcription of RXR α and NF- κ B were evaluated. Compound **6** showed intriguing transcriptional inhibitory activities on both RXR α and NF- κ B, indicating this compound may have anti-cancer properties.

4. Experimental

4.1. General experimental procedures

Optical rotations were measured with a Rudolph Autopol IV/IV-T automatic polarimeter (NJ, USA). UV spectra were recorded on a Shimadzu UV-2600 UV-visible spectrophotometer (Shimadzu, Japan). IR spectra were obtained on a Bruker ALPHA FT-IR spectrometer (Bruker, Germany) with KBr pellets. NMR spectra were acquired on Bruker Avance 600III spectrometers (Bruker, Germany) with tetramethylsilane as the internal standard, using methanol- d_4 or pyridine- d_5 as solvents. HRESIMS experiments were conducted on a Thermo Scientific Q Exactive Quadrupole-Orbitrap mass spectrometer (Thermo, USA). ECD spectra were acquired on a Jasco J-810 circular dichroism spectrometer (Jasco, Japan) in methanol. Column chromatography separations were performed on silica gel (200–300 mesh, Qingdao Marine Chemical Inc., Qingdao, People's Republic of China), Sephadex LH-20 (Amersham Pharmacia Biotech, Sweden), and ODS (YMC, Japan). Analytical HPLC separations were performed with a Shimadzu LC-20AT pump system (Shimadzu, Japan) with a DAD, and semipreparative separations were performed with a Shimadzu LC-8A pump system (Shimadzu, Japan) with a DAD. Fractions were monitored by TLC (Qingdao Marine Chemical Inc., Qingdao, People's Republic of China) and visualized under a UV lamp at 254 nm or 365 nm after

spraying with 5% H₂SO₄ in ethanol, followed by heating.

4.2. Plant material

Tender stems of *Vernonia amygdalina* Delile (compositae) were collected from Taiwan, China, in April 2016, and authenticated by Professor Zhenji Li, College of the Environment Ecology, Xiamen University. A voucher specimen (VA-308201604) has been deposited in the School of Pharmaceutical Sciences, Xiamen University.

4.3. Extraction and isolation

The dried, powdered tender stems of *Vernonia amygdalina* Del. (5.5 kg) were soaked overnight in 40 L of 60% EtOH, then refluxed three times in 60% EtOH for 2.5 hours each time. Concentrating the filtrate under reduced pressure yielded crude extract (1073 g), and then the crude extract was suspended in water and partitioned successively with petroleum ether (3 × 4 L), CH₂Cl₂ (3 × 4 L), EtOAc (3 × 4 L) and *n*-BuOH (3 × 4 L). After removing the solvent, the CH₂Cl₂ extract (97 g) was separated by silica gel column chromatography eluted with a gradient of CH₂Cl₂-CH₃OH (100:0 → 80:20, v/v) to yield eleven fractions (Fr. 1–11). Fr. 4 (3.5 g) was subjected to a Sephadex LH-20 column (MeOH) and then separated on a silica gel column eluted with CH₂Cl₂-(CH₃)₂CO (100:1 → 5:1, v/v) to yield ten fractions (Fr. 4.1–4.10). Among them, Fr. 4.5 (300.9 mg) was successively separated by a Sephadex LH-20 column (MeOH) and an ODS column [CH₃OH-H₂O (15:85 → 100:0, v/v)], and finally purified by prep-HPLC (CH₃OH-H₂O, 80:20, v/v) to afford compound **1** (2 mg). Fr. 8 (16.2 g) was further separated by silica gel column chromatography [CH₂Cl₂-CH₃OH (99:1 → 80:20, v/v)] to yield nine fractions (Fr. 8.1–8.9). Then Fr. 8.8 (12.7 g) was separated into twelve fractions (Fr. 8.8.1–8.8.12) by ODS column chromatography [CH₃OH-H₂O (50:50, v/v)] and Fr. 8.8.3 (588.8 mg) was purified by repeated prep-HPLC [CH₃OH-H₂O (60:40, v/v)] separations to afford compounds **3** (6.0 mg), **7** (10.7 mg) and **8** (1.9 mg). Fr. 8.8.5 (664.5 mg) separated by prep-HPLC [CH₃OH-H₂O (60:40, v/v); CH₃CN-H₂O (35:65, v/v)] to yield **9** (26.9 mg), **10** (5.2 mg) and **13** (32.8 mg). Furthermore, Fr. 8.8.7 (195.0 mg) was purified by repeated prep-HPLC [CH₃OH-H₂O (60:40, v/v)] separations to afford **4** (2.8 mg) and **5** (2.5 mg). Fr. 8.8.8 (195.0 mg) was purified by prep-HPLC with [CH₃OH-H₂O (60:40, v/v) to afford **2** (30.3 mg) and by prep-HPLC with [CH₃CN-H₂O (35:65, v/v)] to obtain **11** (5.0 mg) and **14** (30.0 mg). Fr. 8.8.12 (271.9 mg) was purified by prep-HPLC [CH₃OH-H₂O (70:30, v/v)] to afford **6** (2.0 mg) and **12** (2.4 mg).

4.3.1. Veramyoside A (1)

Amorphous white powder; [α]_D²⁵-40.00 (c 1.30, CH₃OH); UV (MeOH) λ_{\max} (log ϵ) 235 (3.41) nm, λ_{\max} (log ϵ) 242 (4.04) nm, λ_{\max} (log ϵ) 250 (4.04) nm; IR (KBr) ν_{\max} 3411, 2962, 2930, 2878, 1738, 1378, 1096, 1053, 1029 cm⁻¹; ECD (MeOH) λ_{\max} ($\Delta\epsilon$) 218 (+0.20) nm, λ_{\max} ($\Delta\epsilon$) 241 (-4.64) nm; ¹H and ¹³C NMR data, see Table 1; positive-ion HRESIMS [M + Na]⁺ m/z 493.2921 (calcd. for C₂₉H₄₂O₅Na, 493.2924).

4.3.2. Veramyoside B (2)

Amorphous white powder; [α]_D²⁵-23.40 (c 4.10, CH₃OH); UV (MeOH) λ_{\max} (log ϵ) 235 (3.21) nm, λ_{\max} (log ϵ) 242 (3.20) nm, λ_{\max} (log ϵ) 250 (2.98) nm; IR (KBr) ν_{\max} 3422, 2937, 2877, 2834, 1725, 1639, 1374, 1076, 1022 cm⁻¹; ECD (MeOH) λ_{\max} ($\Delta\epsilon$) 219 (+3.50) nm, λ_{\max} ($\Delta\epsilon$) 242 (-8.80) nm; ¹H and ¹³C NMR data, see Table 1; positive-ion HRESIMS [M + Na]⁺ m/z 655.3442 (calcd. for C₃₅H₅₂O₁₀Na, 655.3453).

4.3.3. Veramyoside C (3)

Amorphous white powder; [α]_D²⁵-21.67 (c 1.20, CH₃OH); UV (MeOH) λ_{\max} (log ϵ) 235 (2.98) nm, λ_{\max} (log ϵ) 242 (2.88) nm, λ_{\max} (log ϵ) 250 (2.69) nm; IR (KBr) ν_{\max} 3422, 2937, 2877, 2834, 1725,

1639, 1374, 1076, 1022 cm⁻¹; ECD (MeOH) λ_{\max} ($\Delta\epsilon$) 219 (+3.50) nm, λ_{\max} ($\Delta\epsilon$) 242 (-8.80) nm; ¹H and ¹³C NMR data, see Table 1; positive-ion HRESIMS [M + Na]⁺ m/z 655.3442 (calcd. for C₃₅H₅₂O₁₀Na, 655.3453).

4.3.4. Veramyoside D (4)

Amorphous white powder; [α]_D^{23.5}-31.02 (c 1.87, CH₃OH); UV (MeOH) λ_{\max} (log ϵ) 235 (3.12) nm, λ_{\max} (log ϵ) 242 (3.09) nm, λ_{\max} (log ϵ) 250 (2.90) nm; IR (KBr) ν_{\max} 3439, 2961, 2926, 2876, 1751, 1712, 1358, 1073, 1028 cm⁻¹; ECD (MeOH) λ_{\max} ($\Delta\epsilon$) 217 (+3.92) nm, λ_{\max} ($\Delta\epsilon$) 242 (-5.03) nm; ¹H and ¹³C NMR data, see Table 1; positive-ion HRESIMS [M + Na]⁺ m/z 653.3215 (calcd. for C₃₅H₅₀O₁₀Na, 653.3296).

4.3.5. Veramyoside E (5)

Amorphous white powder; [α]_D^{23.4}-31.14 (c 1.67, CH₃OH); UV (MeOH) λ_{\max} (log ϵ) 235 (2.83) nm, λ_{\max} (log ϵ) 242 (2.86) nm, λ_{\max} (log ϵ) 250 (2.67) nm; IR (KBr) ν_{\max} 3439, 2961, 2926, 2878, 1753, 1711, 1364, 1076, 1029 cm⁻¹; ECD (MeOH) λ_{\max} ($\Delta\epsilon$) 222 (+4.98) nm, λ_{\max} ($\Delta\epsilon$) 241 (-4.90) nm; ¹H and ¹³C NMR data, see Table 2; positive-ion HRESIMS [M + Na]⁺ m/z 653.3204 (calcd. for C₃₅H₅₀O₁₀Na, 653.3296).

4.3.6. Veramyoside F (6)

Amorphous white powder; [α]_D^{23.99}9.02 (c 1.33, CH₃OH); UV (MeOH) λ_{\max} (log ϵ) 235 (3.11) nm, λ_{\max} (log ϵ) 242 (3.10) nm, λ_{\max} (log ϵ) 250 (2.90) nm; IR (KBr) ν_{\max} 3439, 2926, 2878, 1753, 1711, 1363, 1077, 1029 cm⁻¹; ECD (MeOH) λ_{\max} ($\Delta\epsilon$) 223 (+4.58) nm, λ_{\max} ($\Delta\epsilon$) 245 (-2.14) nm; ¹H and ¹³C NMR data, see Table 2; positive-ion HRESIMS [M + Na]⁺ m/z 653.3299 (calcd. for C₃₅H₅₀O₁₀Na, 653.3296).

4.3.7. Veramyoside G (7)

Amorphous white powder; [α]_D^{23.7}-17.98 (c 1.78, CH₃OH); UV (MeOH) λ_{\max} (log ϵ) 235 (3.18) nm, λ_{\max} (log ϵ) 242 (3.17) nm, λ_{\max} (log ϵ) 250 (2.96) nm; IR (KBr) ν_{\max} 3440, 2931, 2882, 1753, 1713, 1362, 1071, 1045 cm⁻¹; ECD (MeOH) λ_{\max} ($\Delta\epsilon$) 223 (+9.62) nm, λ_{\max} ($\Delta\epsilon$) 244 (-4.92) nm; ¹H and ¹³C NMR data, see Table 2; positive-ion HRESIMS [M + Na]⁺ m/z 669.3250 (calcd. for C₃₅H₅₀O₁₀Na, 669.3245).

4.3.8. Veramyoside H (8)

Amorphous white powder; [α]_D^{23.8}-36.22 (c 1.27, CH₃OH); UV (MeOH) λ_{\max} (log ϵ) 235 (3.40) nm, λ_{\max} (log ϵ) 242 (3.39) nm, λ_{\max} (log ϵ) 250 (3.19) nm; IR (KBr) ν_{\max} 3440, 2964, 2935, 2879, 1753, 1709, 1358, 1077 cm⁻¹; ECD (MeOH) λ_{\max} ($\Delta\epsilon$) 223 (+6.95) nm, λ_{\max} ($\Delta\epsilon$) 245 (-5.08) nm; ¹H and ¹³C NMR data, see Table 2; positive-ion HRESIMS [M + Na]⁺ m/z 669.3249 (calcd. for C₃₅H₅₀O₁₀Na, 669.3245).

4.3.9. Veramyoside H (9)

Amorphous white powder; [α]_D^{23.7}52.63 (c 1.33, CH₃OH); UV (MeOH) λ_{\max} (log ϵ) 235 (2.69) nm, λ_{\max} (log ϵ) 242 (2.74) nm, λ_{\max} (log ϵ) 250 (2.55) nm; IR (KBr) ν_{\max} 3505, 3413, 2951, 2930, 2906, 1758, 1709, 1353, 1086, 1042 cm⁻¹; ECD (MeOH) λ_{\max} ($\Delta\epsilon$) 241 (+1.00) nm, λ_{\max} ($\Delta\epsilon$) 298 (-0.89) nm; ¹H and ¹³C NMR data, see Table 3; negative-ion HRESIMS [M-H]⁻ m/z 645.3304 (calcd. for C₃₅H₄₉O₁₁, 645.3269).

4.3.10. Veramyoside I (10)

Amorphous white powder; [α]_D^{25.0}12.77 (c 1.41, CH₃OH); UV (MeOH) λ_{\max} (log ϵ) 235 (2.66) nm, λ_{\max} (log ϵ) 242 (2.69) nm, λ_{\max} (log ϵ) 250 (2.52) nm; IR (KBr) ν_{\max} 3501, 3413, 2950, 2906, 2882, 1756, 1709, 1359, 1088, 1025 cm⁻¹; ECD (MeOH) λ_{\max} ($\Delta\epsilon$) 239 (+2.86) nm; ¹H and ¹³C NMR data, see Table 3; positive-ion HRESIMS [M + Na]⁺ m/z 671.3315 (calcd. for C₃₅H₅₂O₁₁ Na, 671.3402).

Table 1
 ^1H (600 MHz) and ^{13}C NMR (150 MHz) Data for Compounds 1–4 (δ in ppm, J in Hz).

No.	1 ^a		2 ^b		3 ^b		4 ^b	
	δ_{C}	δ_{H}	δ_{C}	δ_{H}	δ_{C}	δ_{H}	δ_{C}	δ_{H}
1 α	36.0	1.34, dd (13.0, 3.5)	35.4	1.23, dd, (13.6, 2.9)	35.3	1.21, overlap	35.3	1.21, m
1 β		1.97, t (3.5)		1.82, overlap		1.80, m		1.80, m
2 α	32.3	1.85, br. d (13.0)	30.5	2.13, m	30.5	2.14, m	30.5	2.13, m
2 β		1.46, br. d (13.0)		1.71, m		1.69, m		1.70, m
3	71.4	3.51, m	77.3	3.98, m	77.3	3.97, m	77.3	3.97, m
4 α	38.5	1.69, m	34.9	2.04, m	34.8	2.02, m	34.9	2.04, m
4 β		1.29, overlap		1.41, q (12.4)		1.39, m		1.41, m
5	40.6	1.42, m	39.5	1.32, m	39.5	1.31, m	39.5	1.31, m
6 α	31.0	1.31, m	30.6	1.82, overlap	30.4	1.80, m	30.5	1.81, m
6 β		1.92, m						
7	121.9	5.46, br. s	121.5	5.38, br. s	122.0	5.33, br. s	121.6	5.37, m
8	137.3		136.6		135.3		136.4	
9	145.5		144.7		144.7		144.7	
10	37.0		36.6		36.6		36.5	
11	119.6	5.53, d (6.5)	119.2	5.49, d (6.0)	118.6	5.44, br. s	119.0	5.44, m
12 α	41.4	2.26, d, (17.3)	41.1	2.48, m	40.8	2.54, d (17.2)	40.9	2.44, m
12 β		2.02, m		2.29, dd (17.4, 6.0)		2.23, m		2.19, m
13	45.0		44.5		44.7		44.6	
14	52.6	2.37, m	51.9	2.34, m	49.8	2.68, m	51.9	2.33, overlap
15 α	24.5	1.93, m	24.1	1.82, m	33.1	2.25, m	24.1	1.85, m
15 β		1.63, m		1.56, dd (11.6, 5.9)		1.93, m		1.55, m
16 α	27.7	2.03, m	27.1	2.01, m	77.9	6.03, t (8.0)	27.1	1.87, m
16 β				1.91, m				
17	47.9	2.65, t, (9.9)	47.7	2.79, t (11.3)	55.0	3.15, d (8.0)	47.6	2.74, t (9.5)
18	13.0	0.47, s	13.1	0.57, s	14.1	0.62, s	13.1	0.54, s
19	19.9	0.91, s	19.8	0.81, s	19.8	0.76, s	19.8	0.80, s
20	134.8		136.6		131.4		136.9	
21	176.5		175.0		174.8		173.9	
22	151.9	7.52, t (1.4)	151.2	7.86, s	152.8	8.05, s	147.5	7.57, overlap
23	84.4	5.33, dd, (1.4, 0.9)	83.8	5.78, s	83.9	5.77, s	83.9	5.65, s
24	79.7		79.5		79.7		85.0	
25	33.3	2.11, quint (7.1)	33.2	2.49, m	33.0	2.47, m	34.2	2.49, m
26	18.7	0.99, d (7.1)	19.2	1.26, d (7.0)	19.0	1.21, d (6.4)	17.6	1.02, d (7.0)
27	18.7	1.03, d (7.1)	19.3	1.26, d (7.0)	19.1	1.21, d (6.4)	17.5	1.21, d (7.0)
28	71.3	3.92, q (6.6)	70.9	4.44, m	70.6	4.41, m	211.3	
29	18.6	1.30, d (6.6)	19.5	1.61, d (6.5)	19.4	1.58, d (6.4)	28.1	2.33, s
16-AcO					171.1			
1'			102.6	5.04, d (7.6)	102.7	5.04, d (8.0)	102.6	5.03, overlap
2'			75.8	4.07, t (7.6)	75.7	4.07, t (8.0)	75.7	4.07, m
3'			79.1	4.32, m	79.1	4.32, m	79.0	4.32, m
4'			72.1	4.29, m	72.1	4.29, m	72.1	4.28, m
5'			78.9	4.01, m	78.9	4.02, m	78.9	4.01, m
6'			63.3	4.60, br. d (11.3)	63.3	4.61, br. d (11.6)	63.3	4.60, d (11.7)
				4.44, m		4.44, m		4.43, dd (11.7, 5.3)

^a Recorded in methanol- d_4 .

^b Recorded in pyridine- d_6 .

4.3.11. Veramyoside J (11)

Amorphous white powder; $[\alpha]_{\text{D}}^{25.7}$ 4.24 (c 3.30, CH_3OH); UV (MeOH) λ_{max} (log ϵ) 235 (3.02) nm, λ_{max} (log ϵ) 242 (3.06) nm, λ_{max} (log ϵ) 250 (2.88) nm; IR (KBr) ν_{max} 3424, 2964, 2934, 2881, 1769, 1729, 1639, 1379, 1250, 1077, 1029 cm^{-1} ; ECD (MeOH) λ_{max} ($\Delta\epsilon$) 243 (+2.53) nm; ^1H and ^{13}C NMR data, see Table 3; positive-ion HRESIMS $[\text{M} + \text{Na}]^+$ m/z 713.3510 (calcd. for $\text{C}_{37}\text{H}_{54}\text{O}_{12}$ Na, 713.3507).

4.4. General procedure for acid hydrolysis determine of the absolute configuration of the sugars

Compound 2 (10.0 mg) was hydrolyzed in 1 M HCl (14.0 mL) by heating at 80 °C for 4 hours. The mixture was extracted with water saturated dichloromethane to remove the nonpolar components. The remaining solution was concentrated and dissolved in pyridine and reacted with L-cysteine methyl ester hydrochloride (5.0 mg) at 60 °C for 1 h. Then, O-tolylisothiocyanate (500 μL) was added, and the mixture was reacted at 60 °C for an additional 1 h. The reaction product was analyzed by HPLC (SilGreen C_{18} 5 μm , 4.6 \times 250 mm; $\text{CH}_3\text{CN}-\text{H}_2\text{O}$

mobile phase (25:75, v/v); detection wavelength of 254 nm; 0.8 mL/min). The sugar in compound 2 was identified as D-glucose in (t_{R} 18.370 min) [authentic samples, D-glucose (t_{R} , 18.325 min) and L-glucose (t_{R} , 16.820 min)].

4.5. Snatzke's method to identify the absolute configuration of the vic-diols in 1

Based on the reported procedure (Bari et al., 2001), the sample and $\text{Mo}_2(\text{OAc})_4$ were mixed in dry DMSO at a ratio of 1:1.25, and the CD spectrum was immediately measured. CD curves were recorded every 10 min until a stationary ICD curve was obtained (after approximately 1 hour). Then, the inherent CD was subtracted, and the Cotton effects at approximately 310 nm and 400 nm were analyzed as the diagnostic bands, and this bands are closely correlated with the absolute configuration of the vic-diol moiety.

Table 2
¹H (600 MHz) and ¹³C NMR (150 MHz) Data for Compounds 5–8 (δ in ppm, J in Hz).

No.	5 ^a		6 ^a		7 ^a		8 ^a	
1α	35.4	1.21, m	35.4	1.24, br. d (13.0)	35.2	1.20, overlap	35.3	1.22, m
1β		1.79, m		1.82, overlap		1.80, m		1.82, overlap
2α	30.5	2.13, m	30.5	2.14, m	30.5	2.12, br. d (11.5)	30.5	2.13, br. d (11.4)
2β		1.70, m		1.70, m		1.68, m		1.69, m
3	77.3	3.96, m	77.3	3.97, m	77.3	3.95, m	77.3	3.96, m
4α	34.9	2.03, m	34.9	2.03, br. d (12.0)	34.8	2.01, br. d (12.0)	34.9	2.02, br. d (12.4)
4β		1.40, m		1.40, q (12.0)		1.39, m		1.39, q (12.4)
5	39.5	1.31, m	39.5	1.31, m	39.4	1.27, m	39.5	1.30, m
6	30.6	1.82, m	30.6	1.81, m	30.4	1.78, m	30.6	1.80, m
7	121.5	5.40, overlap	121.6	5.38, br. s	121.7	5.39, overlap	121.7	5.41, br. s
8	135.6		136.5		135.8		136.0	
9	144.7		144.8		144.6		144.8	
10	36.6		36.6		36.5		36.6	
11	119.1	5.41, overlap	119.1	5.49, br. d (5.5)	118.7	5.40, overlap	118.8	5.48, br. d (6.1)
12α	40.7	2.44, overlap	40.9	2.44, overlap	40.9	2.54, d (17.0)	41.0	2.50, overlap
12β		2.14, m		2.30, dd (17.0,5.5)		2.07, dd (17.0, 6.6)		2.34, m
13	44.7		44.7		44.9		45.3	
14	52.0	2.37, m	51.9	2.33, m	50.2	2.91, t (8.6)	49.9	2.91, t (8.6)
15α	24.2	1.87, m	24.2	1.82, overlap	35.9	2.24, m	36.2	2.29, m
15β		1.62, m		1.58, m				2.25, m
16α	27.7	1.95, m	26.9	2.12, m	76.0	5.01, overlap	74.3	5.35, t (7.2)
16β				1.94, m				
17	47.3	2.81, t (9.7)	47.8	2.77, t, (9.7)	58.5	3.19, d (7.5)	59.5	3.15, d (7.1)
18	12.8	0.76, s	13.1	0.58, s	14.2	0.65, s	14.4	0.71, s
19	19.8	0.80, s	19.8	0.80, s	19.7	0.78, s	19.8	0.79, s
20	136.6		136.3		136.0		134.7	
21	174.7		174.4		174.4		174.7	
22	147.3	7.31, s	147.9	7.42, s	147.5	7.73, s	148.8	7.57, overlap
23	85.2	5.60, s	85.1	5.71, s	84.0	5.38, m	85.2	5.66, s
24	85.6		85.9		84.8		85.8	
25	36.0	2.46, overlap	35.8	2.51, m	33.9	2.46, m	35.7	2.47, overlap
26	17.6	1.16, d (6.5)	17.6	1.19, d (6.8)	17.3	1.17, d (6.8)	18.1	1.13, d (7.0)
27	18.1	1.15, d (6.5)	18.1	1.16, d (6.8)	17.4	0.95, d (6.8)	17.6	1.17, d (7.0)
28	213.3		213.2		211.3		213.0	
29	29.5	2.44, s	29.4	2.47, s	28.2	2.32, s	29.3	2.42, s
1'	102.7	5.03, overlap	102.7	5.04, d (7.7)	102.6	5.02, overlap	102.7	5.03, d (8.0)
2'	75.7	4.06, m	75.8	4.07, m	75.7	4.05, t (7.5)	75.8	4.06, t (8.0)
3'	79.0	4.32, m	79.1	4.32, m	79.0	4.29, m	79.1	4.31, m
4'	72.1	4.28, m	72.1	4.29, m	72.1	4.28, m	72.1	4.28, m
5'	78.9	4.00, m	78.9	4.01, m	78.9	3.99, m	78.9	4.01, m
6'	63.3	4.59, d (11.2)	63.3	4.60, br. d (10.4)	63.2	4.58, d (11.6)	63.3	4.60, d (11.2)
		4.43, m		4.43, m		4.41, m		4.43, dd (11.2, 4.6)

^a Recorded in pyridine-*d*₆.

4.6. Preparation of the (S)-MTPA (**1a**) and (R)-MTPA (**1b**) esters

Under the protection of nitrogen in NMR tubes, portions of **1** (0.5 mg) were dissolved in pyridine-*d*₅ and separately reacted with (S)-MTPA chloride (10 μL) and (R)-MTPA chloride (10 μL). The mixtures were completely reacted at room temperature for 3–4 h to prepare the (R)-MTPA ester (**1b**) and the (S)-MTPA ester (**1a**), respectively.

4.7. Quantum chemical ECD calculation method

Monte Carlo conformational searches were carried out by means of the Spartan's 9 software using the merck molecular force field (MMFF). The conformers with a Boltzmann-population of over 5% were chosen for ECD calculations, and the conformers were initially optimized at the B3LYP/6-31 + g (d, p) level in MeOH using the conductor-like polarizable continuum model (CPCM). The theoretical calculations of the ECD curves were carried out MeOH using time-dependent density functional theory (TD-DFT) at the B3LYP/6-311 + g (d, p) level for all conformers of compounds **4**, **9** and **10**. Rotatory strengths for a total of 50 excited states were calculated. ECD spectra were generated using the program SpecDis 1.6 (University of Würzburg, Würzburg, Germany) and GraphPad Prism 5 (University of California San Diego, USA) from dipole-length rotational strengths by applying Gaussian band shapes with sigma = 0.3 eV.

4.8. RXRα transcriptional activities

The RXRα transcriptional activities of the isolates were evaluated by a dual-luciferase reporter assay. 293T cells were seeded at a density of 1 × 10⁴ cells per well in 96-well plates. Then, the cells were transfected with pGL5 luciferase reporter vector (30 ng/mL) and pGAL4-RXRα-LBD vector (15 μg/mL) by Liposome 2000. After 12 hours, the cells were incubated with 9-cis and the test compounds (50 μM) for 12 hours. The luciferase activities were measured using the Dual-Luciferase Assay System Kit (Promega) (Kotani et al., 2010).

$$\text{Relative luciferase activity (\%)} = \text{FL/RL} \times 100\%$$

4.9. NF-κB transcriptional-inhibitory activities

The 293T cells were plated into 96-well plates at a concentration of 1 × 10⁴ cells per well, and then the pGL4.32[luc2P/NF-KB-RE/Hygro] vector (30 μg/mL) and pC-DNA-Rellina vector (15 ng/mL) were co-transfected into the 293T cells. Twelve hours later, the test compounds (50 μM) and TNF-α were added, and the cells were incubated for an additional 6 hours. Then, the activities of Firefly luciferase (FL) and Rellina luciferase (RL) were determined using the Dual-Luciferase Reporter Assay System Kit (Promega).

$$\text{Relative luciferase activity (\%)} = \text{FL/RL} \times 100\%.$$

Table 3
 ^1H (600 MHz) and ^{13}C NMR (150 MHz) Data for Compounds 9–12 (δ in ppm, J in Hz).

No.	9 ^a		10 ^a		11 ^a		12 ^a	
	δ_{C}	δ_{H}	δ_{C}	δ_{H}	δ_{C}	δ_{H}	δ_{C}	δ_{H}
1 α	35.2	1.24, m	35.3	1.20, m	35.4	1.19, t (13.2)	35.4	1.21, overlap
1 β		1.85, br. d (13.3)		1.81, m		1.80, m		1.82, overlap
2 α	30.4	2.16, m	30.6	2.12, m	30.6	2.13, m	30.6	2.13, overlap
2 β		1.72, m		1.70, m		1.68, m		1.70, m
3	77.3	3.98, m	77.3	3.95, m	77.4	3.94, m	77.3	3.97, m
4 α	34.8	2.04, br. d (12.0)	34.9	2.01, m	34.9	1.99, m	34.9	2.03, br. d (11.0)
4 β		1.40, q (12.0)		1.40, m		1.37, m		1.40, q (11.0)
5	39.5	1.28, m	39.5	1.28, m	39.6	1.28, m	39.5	1.32, m
6	30.4	1.77, m	30.5	1.80, m	30.5	1.76, m	30.5	1.81, overlap
7	123.0	5.25, br. s	121.3	5.38, br. s	122.0	5.28, s	121.6	5.37, br. s
8	133.8		135.6		135.4		136.5	
9	145.1		144.5		144.7		144.7	
10	36.7		36.5		36.6		36.6	
11	118.1	5.52, br. d (5.7)	119.1	5.48, br. d (6.0)	118.7	5.44, d (5.5)	119.1	5.42, br. d (5.6)
12 α	40.3	2.40, m	41.7	2.73, dd (17.5, 6.0)	41.2	2.54, m	40.8	2.44, overlap
12 β		2.28, m		2.27, d (17.5)		2.24, m		2.11, overlap
13	41.3		43.6		43.4		44.5	
14	46.5	2.60, m	49.6	2.78, m	49.3	2.52, m	52.0	2.36, overlap
15 α	38.0	2.40, m	36.4	2.12, m	33.5	2.11, m	24.1	1.86, m
15 β		2.12, m				1.84, m		1.58, m
16 α	214.6		75.0	4.59, br. d (9.8)	77.4	5.53, t (7.8)	27.7	1.96, m
16 β								1.90, m
17	63.1	3.00, br. s	60.6	2.43, overlap	56.6	2.50, m	47.4	2.77, t (9.3)
18	14.4	0.66, s	14.2	0.72, s	14.1	0.63, s	13.0	0.57, s
19	19.8	0.80, s	19.8	0.83, s	19.9	0.76, s	19.8	0.80, s
20	38.2	3.09, m	40.7	3.10, m	40.0	3.08, m	136.7	
21	178.4		178.9		178.5		173.9	
22	27.4	2.87, q (10.8)	28.5	3.11, m	27.9	2.70, m	147.3	
		2.31, m		2.42, overlap		2.24, m		7.51, s
23	81.6	5.12, q (5.6)	81.4	5.15, m	81.4	5.05, overlap	83.9	5.50, br. s
24	84.6		84.8		84.8		84.9	
25	35.7	2.49, m	35.6	2.43, overlap	35.6	2.37, m	33.9	2.47, m
26	18.0	1.19, d (7.0)	18.0	1.16, d (7.0)	18.0	1.10, d (6.6)	17.5	0.99, d (6.8)
27	17.9	1.14, d (7.0)	18.0	1.15, d (7.0)	17.9	1.10, d (6.6)	17.5	1.20, d (6.8)
28	213.8		214.2		214.3		211.3	
29	30.0	2.45, s	30.2	2.44, s	30.3	2.43, s	28.3	2.33, s
16-AcO						171.2		
					21.5	2.00, s		
1'	102.7	5.05, d (7.8)	102.7	5.05, overlap	102.8	5.00, overlap	102.7	5.04, d (7.7)
2'	75.8	4.08, t (7.8)	75.7	4.05, m	75.8	4.04, t (7.6)	75.8	4.06, m
3'	79.1	4.32, m	79.0	4.30, m	79.1	4.28, m	79.1	4.31, m
4'	72.1	4.29, m	72.1	4.28, m	72.2	4.26, m	72.1	4.28, m
5'	78.9	4.01, m	78.9	4.00, m	79.0	3.99, m	78.9	4.01, m
6'	63.3	4.61, d (11.5)	63.3	4.59, br. d (10.0)	63.4	4.57, d (11.8)	63.3	4.60, br. d (11.0)
		4.43, m		4.42, dd (10.0, 5.1)		4.40, dd (11.8, 4.0)		4.44, m

^a Recorded in pyridine-*d*₆.

Conflicts of interest

The authors declare no competing financial interest.

Author contributions

||Xiangzhong Liu and Wenjing Tian contributed equally to this research.

Acknowledgment

This study was supported by Fundamental Research Funds for the Central Universities (20720160117 and 20720150204) and Xiamen Science and Technology program grant (No. 3502Z20161235 and 3502Z20173021).

Appendix A. Supplementary data

Supplementary data to this article can be found online at <https://doi.org/10.1016/j.phytochem.2018.10.036>.

References

- Audu, S.A., Taiwo, A.E., Ojuolape, A.R., 2012. A study review of documented phytochemistry of *vernonia amygdalina* (family asteraceae) as the basis for pharmacologic activity of plant extract. *J. Nat. Sci. Res.* 2 (7).
- Bari, L.D., Pescitelli, G., Pratelli, C., Dario Pini, A., Salvadori, P., 2001. Determination of absolute configuration of acyclic 1,2-diols with Mo2(OAc)4. 1. Sznatzke's method revisited. *J. Org. Chem.* 66, 4819–4825.
- Bloch, K., 1965. The biological synthesis of cholesterol. *Science* 150, 19.
- Cao, X., Liu, W., Lin, F., Li, H., Kolluri, S.K., Lin, B., Han, Y.H., Dawson, M.I., Zhang, X.K., 2004. Retinoid X receptor regulates Nur77/TR3-dependent apoptosis [corrected] by modulating its nuclear export and mitochondrial targeting. *Mol. Cell. Biol.* 24, 9705.
- Croft, M., Benedict, C.A., Ware, C.F., 2013. Clinical targeting of the TNF and TNFR superfamilies. *Nat. Rev. Drug Discov.* 12, 147–168.
- Dolcet, X., Llobet, D., Pallares, J., Matias-Guiu, X., 2005. NF- κ B in development and progression of human cancer. *Virchows Arch.* 446, 475–482.
- Igile, G.O., Oleszek, W., Jurzysta, Aquino, R., Tommasi, N., Pizzi, C., 1995. Vernonioides D and E, two novel saponins from *Vernonia amygdalina* Del. (Compositae). *J. Nat. Prod.* 589, 1438–1443.
- Jisaka, M., Ohigashi, H., Takagaki, T., Nozaki, H., Tada, T., Hirota, M., Irie, R., Huffman, M.A., Nishida, T., Kaji, M., 1992. Bitter steroid glucosides, vernonioides A 1, A 2, and A 3, and related B 1 from a possible medicinal plant, *Vernonia amygdalina*, used by wild chimpanzees. *Cheminform* 48, 625–632.
- Jisaka, M., Ohigashi, H., Takegawa, K., Hirota, M., Irie, R., Huffman, M.A., Koshimizu, K., 1993. Steroid glucosides from *vernonia amygdalina*, a possible chimpanzee medicinal plant. *Phytochemistry* 34, 409–413.

- Kamperdick, C., Breitmaier, E., Radloff, M.A.V., 1992. Ein neues Steroidsaponin aus *Vernonia amygdalina* (Compositae). *Adv. Synth. Catal.* 334.
- Kotani, H., Tanabe, H., Mizukami, H., Makishima, M., Inoue, M., 2010. Identification of a naturally occurring rexinoid, honokiol, that activates the retinoid x receptor. *J. Nat. Prod.* 27, 1332–1336.
- Kupchan, S.M., Hemingway, R.J., Karim, A., et al., 1969. Tumor inhibitors. XLVII. Vernodalin and vernomygdin, two new cytotoxic sesquiterpene lactones from *Vernonia amygdalina* del. *J. Org. Chem.* 34 (34), 3908–3911.
- Liu, J., Du, D., Si, Y., Lu, H., Wu, X., Li, Y., Liu, Y., Yu, S., 2010. Application of dimolybdenum reagent $\text{Mo}_2(\text{OAc})_4$ for determination of the absolute configurations of vic-diols. *Chin. J. Org. Chem.* 30, 1270–1278.
- Luo, X., Jiang, Y., Fronczek, F.R., et al., 2011. Isolation and structure determination of a sesquiterpene lactone (vernodalinol) from *Vernonia amygdalina* extracts. *Pharmaceut. Biol.* 49 (5), 464–470.
- Ma, G.X., Feng, W., Sun, Z.H., Li, P.F., Zhu, N.L., Yang, J.S., Xu, X.D., Wu, H.F., 2016. New stigmastane type of steroidal glycosides from the roots of *Vernonia cumingiana*. *J. Carbohydr. Chem.* 35, 172–179.
- Marcin, Górecki, Jabłońska, Ewa, Anna, Kruszevska, Suszczyńska, Agata, Urbańczykowska, Zofia, Gerards, Michael, Morzycki, J.W., Szczepek, W.J., Frelek, Jadwiga, 2007. Practical method for the absolute configuration assignment of tert/tert 1,2-diols using their complexes with $\text{Mo}_2(\text{OAc})_4$. *J. Org. Chem.* 72, 2906–2916.
- Nerdy, 2015. In silico study of sesquiterpene lactone compounds from South Africa leaves (*Vernonia amygdalina* Del.) as antimalarial and anticancer. *Int. J. Pharmtech. Res.* 7 (1), 47–53.
- Niu, B., Ke, C.Q., Li, B.H., Li, Y., Yi, Y., Luo, Y., Shuai, L., Yao, S., Lin, L.G., Li, J., 2017. Cucurbitane glucosides from the crude extract of *siraitia grosvenorii* with moderate effects on PGC-1 α promoter activity. *J. Nat. Prod.* 80.
- Ohtani, I., Kusumi, T., Kashman, Y., Kakisawa, H., 1991. High-field FT NMR application of Mosher's method. The absolute configurations of marine terpenoids. *Cheminform* 22, 4092–4096.
- Ohigashi, H., Jisaka, M., Takagaki, T., Nozaki, H., Tada, T., Huffman, M.A., Nishida, T., Kaji, M., Koshimizu, K., 1991. Bitter principle and a related steroid glucoside from *vernonia amygdalina*, a possible medicinal plant for wild chimpanzees. *J. Agric. Chem. Soc. Jpn.* 55, 1201–1203.
- Quasie, O., Zhang, Y.M., Zhang, H.J., Luo, J., Kong, L.Y., 2016. Four new steroid saponins with highly oxidized side chains from the leaves of *Vernonia amygdalina*. *Phytochem. Lett.* 15, 16–20.
- Schmittmann, T., Rotscheidt, K., Breitmaier, E., 1994. Drei Neue Steroidsaponine aus *Vernonia amygdalina* (Compositae). *Adv. Synth. Catal.* 336.
- Tanaka, T., Nakashima, T., Ueda, T., Tomii, K., Kouno, I., 2007. Facile discrimination of aldose enantiomers by reversed-phase HPLC. *Chem. Pharmaceut. Bull.* 55, 899–901.
- Tian, W., Qiu, Y., Jin, X.J., Chen, H., Yao, X., Dai, Y., Yao, X.S., 2016. Hypersampsones S-W, new polycyclic polyprenylated acylphloroglucinols from *Hypericum sampsonii*. *RSC Adv.* 6, 50887–50894.
- Wang, J., Song, H., Wu, X., Zhang, S., Gao, X., Li, F., Zhu, X., Chen, Q., 2018. Steroidal saponins from *vernonia amygdalina* Del. and their biological activity. *Molecules* 23, 579.
- Ye, X.S., He, J., Cheng, Y.C., Zhang, L., Qiao, H.Y., Pan, X.G., Zhang, J., Liu, S.N., Zhang, W.K., Xu, J.K., 2017. Cornusides a–O, bioactive iridoid glucoside dimers from the fruit of *cornus officinalis*. *J. Nat. Prod.* 80 (12).
- Yedjou, C.G., Tchounwou, P.B., 2017. Abstract 4083: basic mechanisms of *Vernonia amygdalina* exert antitumor activities in breast cancer cells. *Cancer Res.* 77 (13 Supplement) 4083–4083.
- Zhang, C., Wen, R., Ma, X.L., Zeng, K.W., Xue, Y., Zhang, P.M., Zhao, M.B., Jiang, Y., Liu, G.Q., Tu, P.F., 2018. Nitric oxide inhibitory sesquiterpenoids and its dimers from *artemisia freyniana*. *J. Nat. Prod.* 81.
- Zhou, Y., Zhao, W., Xie, G., Huang, M., Hu, M., Jiang, X., Zeng, D., Liu, J., Zhou, H., Chen, H., 2014. Induction of Nur77-dependent apoptotic pathway by a coumarin derivative through activation of JNK and p38 MAPK. *Carcinogenesis* 35, 2660–2669.
- Zeng, Z., Sun, Z., Huang, M., Zhang, W., Liu, J., Chen, L., Chen, F., Zhou, Y., Lin, J., Huang, F., 2015. Nitrostyrene derivatives act as RXR α ligands to inhibit TNF α activation of NF- κ B. *Cancer Res.* 75, 2049–2060.